doi:10.1093/brain/awp114 Brain 2009: 132; 1656–1668 | 1656

BRAIN
A JOURNAL OF NEUROLOGY

Defining Meyer's loop–temporal lobe resections, visual field deficits and diffusion tensor tractography

M. Yogarajah,[1] N. K. Focke,[2] S. Bonelli,[1] M. Cercignani,[3] J. Acheson,[4] G. J. M. Parker,[5] D. C. Alexander,[6] A. W. McEvoy,[7] M. R. Symms,[1] M. J. Koepp[1] and J. S. Duncan[1]

1 Department of Clinical and Experimental Epilepsy, UCL Institute of Neurology and National Society for Epilepsy, UCL, London, UK
2 Department of Clinical Neurophysiology, Georg-August University Goettingen, Goettingen, Germany
3 Department of Neuroimaging, Fondazione Santa Lucia, Rome, Italy
4 Department of Neuro-ophthalmology, National Hospital for Neurology and Neurosurgery, London, UK
5 Imaging Science and Biomedical Engineering, University of Manchester, Manchester, UK
6 Department of Computer Science, UCL, London, UK
7 Department of Neurosurgery, National Hospital for Neurology and Neurosurgery, London, UK

Correspondence to: Prof. J. S. Duncan,
Department of Clinical and Experimental Epilepsy,
UCL Institute of Neurology,
Queen Square,
London WC1N 3BG, UK
E-mail: j.duncan@ion.ucl.ac.uk

Anterior temporal lobe resection is often complicated by superior quadrantic visual field deficits (VFDs). In some cases this can be severe enough to prohibit driving, even if a patient is free of seizures. These deficits are caused by damage to Meyer's loop of the optic radiation, which shows considerable heterogeneity in its anterior extent. This structure cannot be distinguished using clinical magnetic resonance imaging sequences. Diffusion tensor tractography is an advanced magnetic resonance imaging technique that enables the parcellation of white matter. Using seed voxels antero-lateral to the lateral geniculate nucleus, we applied this technique to 20 control subjects, and 21 postoperative patients. All patients had visual fields assessed with Goldmann perimetry at least three months after surgery. We measured the distance from the tip of Meyer's loop to the temporal pole and horn in all subjects. In addition, we measured the size of temporal lobe resection using postoperative T_1-weighted images, and quantified VFDs. Nine patients suffered VFDs ranging from 22% to 87% of the contralateral superior quadrant. In patients, the range of distance from the tip of Meyer's loop to the temporal pole was 24–43 mm (mean 34 mm), and the range of distance from the tip of Meyer's loop to the temporal horn was −15 to +9 mm (mean 0 mm). In controls the range of distance from the tip of Meyer's loop to the temporal pole was 24–47 mm (mean 35 mm), and the range of distance from the tip of Meyer's loop to the temporal horn was −11 to +9 mm (mean 0 mm). Both quantitative and qualitative results were in accord with recent dissections of cadaveric brains, and analysis of postoperative VFDs and resection volumes. By applying a linear regression analysis we showed that both distance from the tip of Meyer's loop to the temporal pole and the size of resection were significant predictors of the postoperative VFDs. We conclude that there is considerable variation in the anterior extent of Meyer's loop. In view of this, diffusion tensor tractography of the optic radiation is a potentially useful method to assess an individual patient's risk of postoperative VFDs following anterior temporal lobe resection.

Keywords: diffusion tensor tractography; Meyer's loop; optic radiation; anterior temporal lobe resection

Received October 23, 2008. Revised March 13, 2009. Accepted March 22, 2009. Advance Access publication May 21, 2009

Abbreviations: ATLR = anterior temporal lobe resection; ML–TH = distance from the tip of Meyer's loop to tip of temporal horn; ML–TP = distance from the tip Meyer's loop to temporal pole; VFD = visual field deficit

Background

Epilepsy is a common, serious, chronic neurological condition. In up to 80% of patients with medial temporal lobe epilepsy (MTLE) associated with hippocampal sclerosis (HS), seizures are refractory to treatment with antiepileptic medications (Semah *et al*., 1998). For this group of patients, anterior temporal lobe resection (ATLR) is a well-established, and effective means of treatment (Wiebe *et al*., 2001). However, this procedure can be complicated by a visual field deficit (VFD), typically a contralateral superior quadrantanopia. This is caused by damage to the anterior portion of the optic radiation, also known as Meyer's loop (Falconer and Wilson, 1958). The reported incidence of postoperative VFDs varies from 68% (Jensen and Seedorff, 1976) to 100% (Barton *et al*., 2005) of patients undergoing ATLRs. In 25–46% of patients the VFD may be severe enough to fail the current visual field criteria set by the UK Driver and Vehicle Licensing Authority (DVLA), even if they are seizure free (Manji and Plant, 2000; Ray *et al*., 2002). This is very significant because most patients cite the ability to drive as one of the five most important factors that would contribute to their complete rehabilitation (Taylor *et al*., 2001). Several factors give rise to the variability in the figures reported in these studies, including the heterogeneity of methods used to assess VFDs (Manji and Plant, 2000), and differences in the nature and extent of surgery (Egan *et al*., 2000). Equally important, is the inter-individual variability in the anatomy and anterior extent of Meyer's loop (Ebeling and Reulen, 1988).

This anatomical heterogeneity cannot be assessed with conventional MRI, because variations in white matter signal are subtle. White matter tracts, such as the optic radiation, cannot therefore be accurately parcellated from surrounding tissue. Diffusion tensor imaging (DTI) is an MRI technique that measures the magnitude of diffusion of water molecules in different directions in each voxel in an image (Basser, 1995). It can be used to probe the microstructure of white matter tracts, and provides the basis for non-invasive diffusion tensor tractography which can map white matter pathways such as the optic radiation (Mori and van Zijl, 2002). Using this technique, we investigated the relationship of Meyer's loop to anatomical landmarks such as the tip of the temporal horn and temporal pole in patients undergoing ATLRs. We also investigated whether these measurements, together with the extent of resection, correlated with the severity of postoperative VFDs.

Methods

Subjects

We studied 21 patients (mean age 37 years, range 18–62 years, 10 males) with medically refractory temporal lobe epilepsy undergoing pre-surgical evaluation at the National Hospital for Neurology and Neurosurgery, London, UK. All patients had undergone structural MRI at 3 Tesla (3T) (Duncan, 1997), and video-EEG had confirmed seizure onset in the medial temporal lobe (MTL) ipsilateral to the clinically defined seizure site. None of these patients had previously used vigabatrin. In 2 of the 11 patients with left-sided temporal lobe epilepsy, structural MRI was normal, and postoperative histopathology confirmed the presence of end folium sclerosis. Of the 10 right temporal lobe epilepsy patients, 2 had anterior temporal lobe cavernomas and 1 also had hippocampal sclerosis. All remaining patients had hippocampal sclerosis identified on MRI ipsilateral to seizure onset, and all patients had a normal, contralateral hippocampus based on qualitative and quantitative MRI criteria (Woermann *et al*., 1998). Postoperative histopathology confirmed the MRI findings in all cases. All patients were taking anti-epileptic medication, and were fluent English language speakers. Handedness was determined using the Edinburgh handedness inventory (Oldfield, 1971), and language dominance was determined using a range of fMRI tasks which have been described previously, and include the use of verbal fluency, and reading tasks (Powell *et al*., 2006). We also studied 20 right-handed, native English speaking, healthy volunteers (mean age 42, range 20–63, 8 males). All controls were left hemisphere language dominant as determined by verbal fluency fMRI tasks.

The study was approved by the National Hospital for Neurology and Neurosurgery and the Institute of Neurology Joint Ethics Committee, and informed written consent was obtained from all subjects. Patient demographics, clinical information and surgical outcome data (based on the ILAE classification of postoperative seizure outcome) (Wieser *et al*., 2001) following epilepsy surgery are listed in Table 1.

Magnetic resonance data

MRI studies were performed on a 3T GE Excite II scanner (General Electric, Wakashua, Milwaukee, WI, USA). Standard imaging gradients with a maximum strength of 40 mT m^{-1} and slew rate 150T $m^{-1}s^{-1}$ were used. All data were acquired using a body coil for transmission, and eight channel phased array coil for reception. The scanning protocol also included a coronal T_1-weighted volumetric acquisition sequence with 1.1-mm thick slices, and hippocampal volumes were determined using a previously described method (Moran *et al*., 1999). High resolution echo planar imaging (HR-EPI) images were also acquired with geometric distortions to match those of the DTI data (Boulby *et al*., 2005).

DTI acquisition

The DTI acquisition sequence was a single-shot spin-echo planar imaging (EPI) sequence, cardiac gated (triggering occurring every QRS complex) (Wheeler-Kingshott *et al*., 2002) with TE = 73 ms. Sets of 60 contiguous 2.4-mm thick axial slices were obtained, covering the whole brain, with diffusion sensitizing gradients applied in each of 52 non-colinear directions [maximum b value of 1200 mm2 s^{-1} ($\delta = 21$ ms, $\Delta = 29$ ms, using full gradient strength of 40 mT m^{-1})] along with six non-diffusion weighted ($b = 0$) scans. The gradient directions were calculated and ordered as described elsewhere (Cook *et al*., 2007). The field of view was 24 cm, and the acquisition matrix size was 96 × 96, zero filled to 128 × 128 during reconstruction so that the reconstructed voxel size was 1.875 mm × 1.875 mm × 2.4 mm.

Table 1 Patient demographics, clinical information and surgical outcome data

Patient No.	Age/ gender	Handedness/ language dominance	Age of epilepsy onset (yrs)	Duration of epilepsy (yrs)	Clinical and EEG diagnosis	Operation	Postoperative outcome (ILAE class)[a]
1	50/M	R/L	16	34	L TLE	L ATLR	5
2	52/M	R/L	6	46	R TLE	R ATLR	1
3	62/F	R/L	1.5	61	L TLE	L ATLR	1
4	48/M	R/L	2.5	45.6	R TLE	R ATLR	1
5	20/F	R/L	11	9	L TLE	L ATLR	1
6	46/F	R/L	7	39	L TLE	L ATLR	3
7	43/F	R/L	12	31	R TLE	R ATLR	3
8	31/M	R/R	2	29	R TLE	R ATLE	1
9	22/F	L/L	10	11	R TLE	R ATLR	1
10	19/F	R/L	1	18	L TLE	L ATLR	3
11	18/F	R/L	3	15	L TLE	L ATLR	1
12	43/M	R/L	1	42	L TLE	L ATLR	1
13	32/F	R/L	4	33	L TLE	L ATLR	1
14	37/F	R/L	7	25	R TLE	R ATLR	1
15	30/F	R/L	18	20	R TLE	R ATLR	1
16	33/F	R/L	7	32	R TLE	R ATLR	[b]
17	34/M	R/L	26	8	L TLE	L ATLR	1
18	43/M	R/L	13	31	L TLE	L ATLR	1
19	36/M	R/L	23	13	L TLE	L ATLR	[b]
20	30/M	R/L	13	17	R TLE	R ATLR	4
21	48/M	R/L	30	18	R TLE	R ATLR[c]	1

a At 12 months follow-up.
b ILAE class 1 at 3 months follow-up (12 month follow-up data not available).
c Modified sparing hippocampus.
M = male; F = female; R = right; L = left.

The DTI acquisition time for a total of 3480 image slices was ~25 min (depending on subject heart rate) and the longest acquisition time was ~35 min in duration. During the acquisition radiographers routinely checked for gross head movement in real time. None of the data used in this study suffered movement artefact of sufficient severity as to warrant exclusion.

DTI processing

All scans were transferred to a Linux based Sun Ultra workstation. The DICOM files of each DTI acquisition were converted into a single multivolume ANALYZE 7.5 file, and were then corrected for eddy currents using the 'eddy-correct' algorithm implemented in FSL v4.1 (http://www.fmrib.ox.ac.uk/fsl/). This tool also conducts an affine registration of every individual volume to the first non-diffusion weighted ($b = 0$) volume, in order to correct for any subtle movement artefact. After this co-registration step, the six $b = 0$ volumes of each subject were extracted and averaged. A multi-tensor model was fitted to the diffusion data using the open source Camino toolkit (http://www.camino.org.uk/) (Cook *et al*., 2006). We used the method of Parker and Alexander to reduce fibre orientation ambiguities in voxels containing fibre crossings (Parker and Alexander, 2003; Parker *et al*., 2003). Voxels in which the single tensor fitted the data poorly were identified using a spherical-harmonic voxel-classification algorithm (Alexander *et al*., 2002). In these voxels a two-tensor model was fitted, and the two principal diffusion directions of the two diffusion tensors provided estimates of the orientations of the crossing fibres. In all other voxels a single tensor model was fitted.

Tractography

The tractography analysis was carried out using the PICo algorithm (Parker *et al*., 2003) extended to multiple fibres as implemented in the Camino package (Parker and Alexander, 2003; Cook *et al*., 2004). Start regions for tractography were based upon previously published work by our group (Ciccarelli *et al*., 2005; Powell *et al*., 2005) (Fig. 1). We used the program MRIcro (http://www.psychology.nottingham.ac.uk), to visualize images and create masks. We identified the lateral geniculate nucleus (LGN) on fractional anisotropy and principal diffusion direction (PDD) maps by selecting the axial slice at the level of the transition from the posterior limb of the internal capsule to the cerebral peduncle (Ciccarelli *et al*., 2005; Bassi *et al*., 2008). At this level part of Meyer's loop could typically be seen on the principal diffusion direction map (Fig. 1). Seed masks, consisting of voxels antero-lateral to the lateral geniculate nucleus at the base of Meyer's loop, with main eigenvectors orientated in an anterior-medial to posterior-lateral orientation, were identified and positioned in white matter from coronal views. Previous studies have shown that probabilistic algorithms can have difficulty in tracking Meyer's loop if seed voxels are placed directly at the lateral geniculate nucleus (Behrens *et al*., 2003). Contiguous voxels, with principal directions in an anterior–posterior direction, were also selected in order to ensure that the entire coronal cross-section of Meyer's loop was encompassed. The volumes of seed masks were standardized for all subjects (15 voxels/127 mm^3). All studies were carried out using 5000 Monte Carlo iterations, an angular threshold of 180° and a fractional anisotropy threshold of 0.1, in order to ensure that the paths detected would not erroneously enter areas of cerebrospinal fluid, and yet had sufficient angular flexibility as to allow tracking of Meyer's loop.

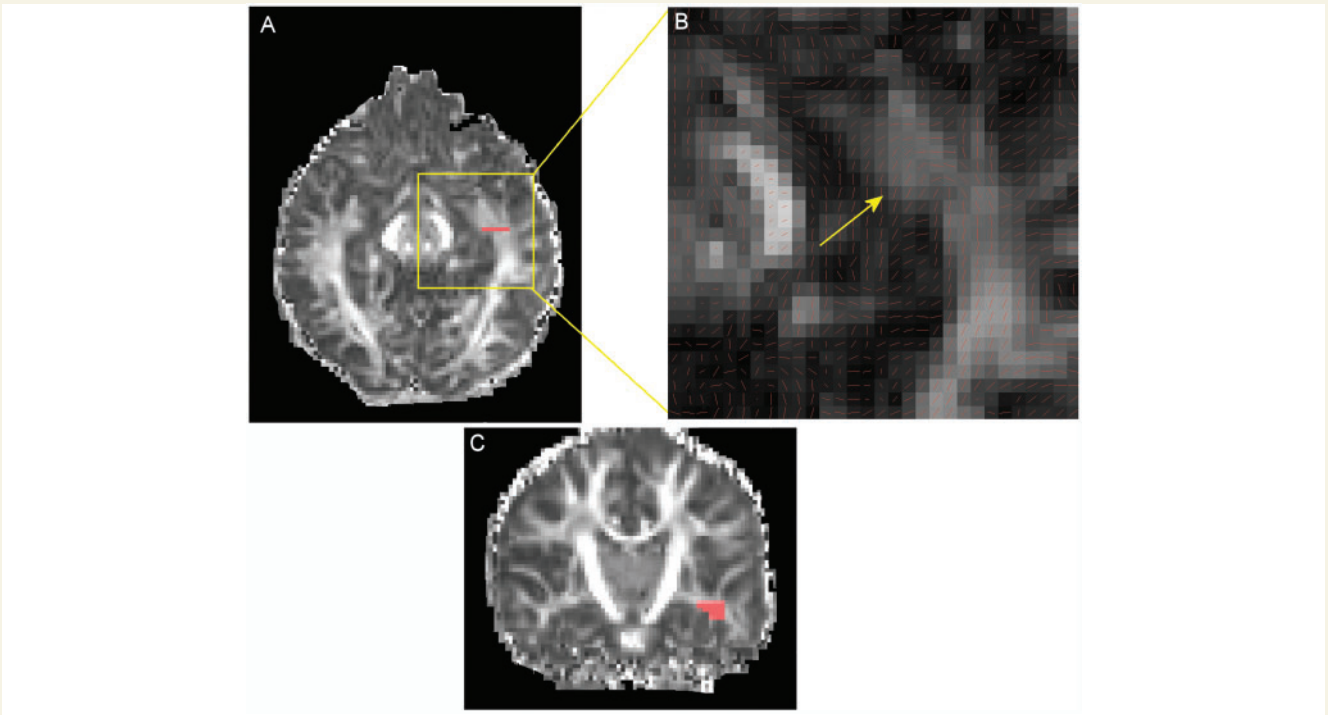

Figure 1 Seed region selection using fractional anisotropy images (seed voxels are shown in red). (**A**) Axial slice where transition from the external limb of the internal capsule to cerebral peduncle is visible. (**B**) Magnified area of axial slice with principle diffusion direction map overlaid on each voxel (red lines). Part of Meyer's loop can be seen clearly (see arrow). (**C**) Seed voxels with principal diffusion direction in anterior-medial to posterior-lateral direction are selected in the corresponding coronal slice at the base of Meyer's loop.

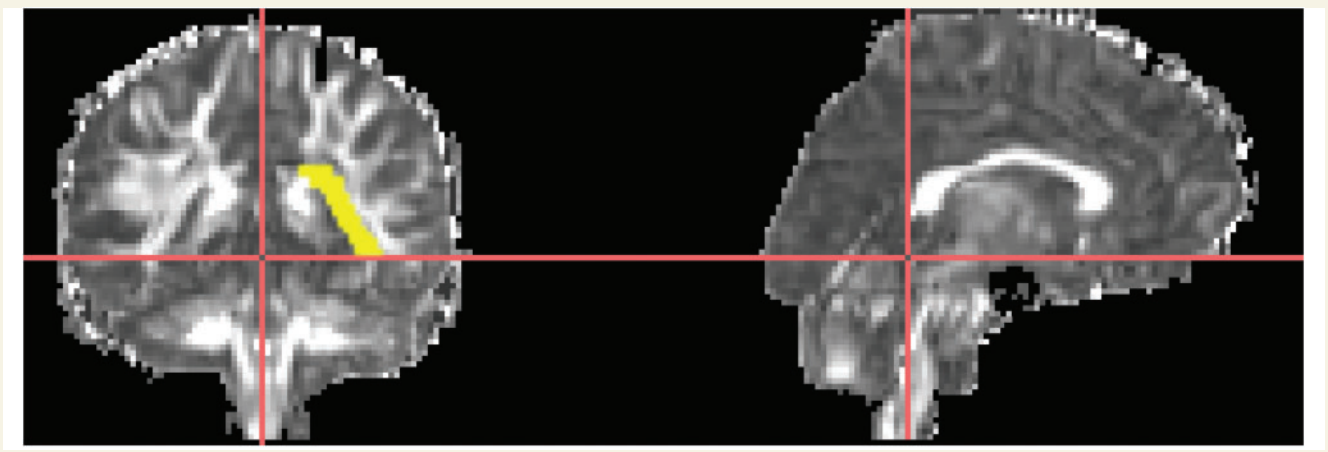

Figure 2 Way point selection using fractional anisotropy images (waypoint voxels are shown in yellow): The coronal slice immediately posterior to splenium of corpus callosum is shown—a way point is superimposed at the level of the occipital horn of the lateral ventricle including the stratum sagittal.

As described in similar studies (Ciccarelli *et al*., 2005; Nilsson *et al*., 2007), we used a way mask to restrict the pathway to the hemisphere ipsilateral to the seed mask, and extended posterior to the splenium of the corpus callosum within the wall of the occipital horn of the lateral ventricle (Fig. 2). It is widely accepted that the optic radiation passes through this region (Burgel *et al*., 1999). All streamlines from the seed region that did not pass through this way point were discarded. In addition, a coronal exclusion mask that included the entire fronto-temporal area was used to remove artefactual connections to neighbouring bundles including the uncinate fasciulus, fronto-occipital fasciculus and anterior commissure (Fig. 3). This is a common problem when probabilistic tractography is applied in regions of adjacent white matter bundles. Rather than placing this mask on the basis of visual discrimination of Meyer's loop from artefactual connections, its coronal position was determined using an objective, iterative process. Tracts were initially generated from the seed region using an exclusion mask

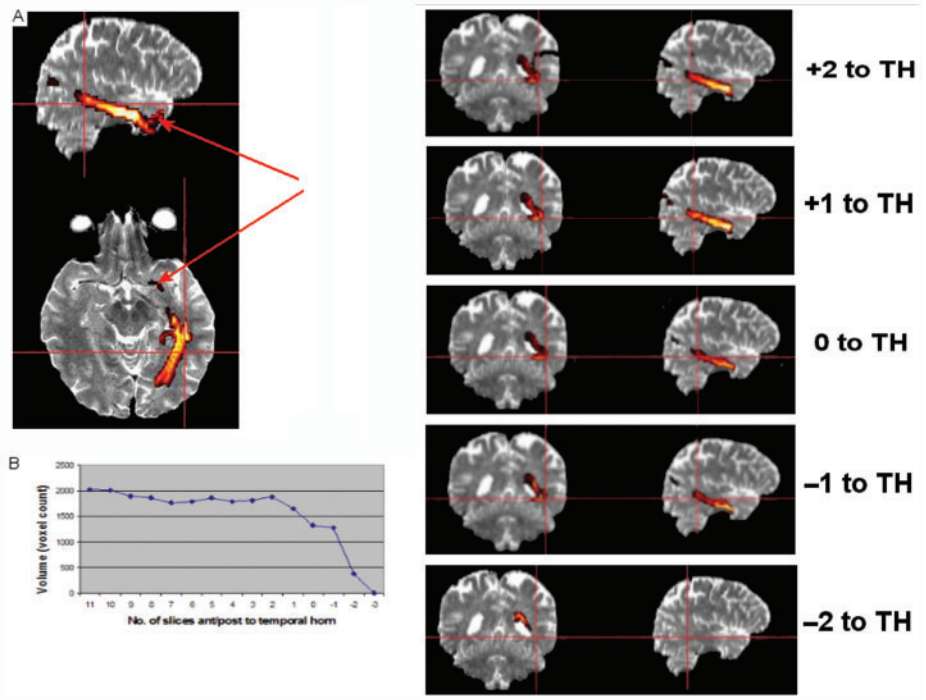

Figure 3 (**A**) Resulting tract without use of fronto-temporal exclusion mask—the red arrow indicates some of the artefactual connections that can arise in areas including the uncinate fasciculus and fronto-occipital fasciculus, making it difficult to estimate the tip of Meyer's loop. (**B**) Iterative tracking using fronto-temporal exclusion mask. All images contain tracts thresholded at the same value and overlaid on distortion matched high-resolution EPI images. The graph is of tract volume against position of exclusion mask ('+' = anterior; '−' = posterior) relative to the tip of the temporal horn (TH). The graph and associated images demonstrate the thinning that occurs in the bulk of the optic radiation once the coronal exclusion mask reaches a coronal position 1 slice anterior to the temporal horn. At this position $\geqslant$10% of the tract volume is lost, and this is chosen as the exclusion mask to be used.

placed 25 mm anterior to the temporal horn. This process was repeated, but in each consecutive trial, the mask was moved posteriorly by one voxel. All streamlines from the seed region that intersected with the exclusion mask were discarded. When this mask coincided with the optic radiation, visible thinning of the estimated trajectory of the optic radiation was evident, and typically coincided with a reduction in tract volume $\geqslant$10%. Therefore, in cases where it was visually difficult to discern thinning with consecutive slices, the mask that first resulted in a reduction in tract volume $\geqslant$10% followed by further, consistent reduction in volume, was chosen as the exclusion mask. This mask was then used in conjunction with the seed and way masks described above (Fig. 3).

Using this method, connectivity distributions were generated from every voxel in the seed mask, and thresholded to include only those with a probability of $\geqslant$5%. This threshold was chosen as it struck a reasonable balance between retaining anatomically valid tracts, and removing obviously artefactual connections. Mask generation and tractography was repeated in 10 randomly selected patients in order to determine the intra-observer variation in the delineation of the anterior extent of the optic radiation. The correlation coefficient was 0.9 which suggested good reproducibility. On repeated analysis by the same observer, the average variation in the anterior extent of Meyer's loop was 2 mm, and the maximum variability was 4 mm. Pre-processing of tractography data, and the tractography itself required ~1 and 6 h, respectively per subject, using a Linux based Sun Ultra workstation.

Quantitative and qualitative analysis

Preoperative mean $b = 0$ images and distortion matched HR-EPI images were co-registered using SPM5 in order to ensure that they were in the same orientation (Wellcome Trust Centre for Imaging Neuroscience, UCL; http://www.fil.ion.ucl.ac.uk/spm). We qualitatively inspected the anatomy of resulting tracts by overlaying them onto the co-registered HR-EPI images. We also assessed the distance between the most anterior extent of Meyer's loop and the temporal pole (ML–TP) and tip of the temporal horn (ML–TH). These landmarks were identified using the preoperative mean $b = 0$ images, with the aid of the distortion matched HR-EPI images.

Resection size estimates

All resections were carried out by a single surgeon (AM) who perfomed a modified Spencer approach. In this approach the lateral ventricles are localized by proceeding from the middle fossa floor up the collateral sulcus. The size of resection was measured using a previously described method, based on the postoperative T_1-weighted images (Barton *et al*., 2005). Using MRIcro to visualize the images, the anterior–posterior extent of resection was estimated by measuring the distance from the anterior tip of the middle cranial fossa formed by the sphenoidal bone fossa (which had previously contained the resected temporal pole) to the posterior margin of the resection. Distances were measured using sagittal images that intersected the

midbrain and lateral wall of the temporal horn, as the optic radiation runs through this region. In the event of resection margins being irregular, we used the most posterior aspect of the resection in the peri-ventricular white matter, which typically also corresponded to the most medial point of resection. In order to compensate for variations in head size and field distortions caused by MRI, the extent of resection was expressed as a fraction of the distance between the anterior tip of the middle sphenoid fossa to the occipital pole (anterior temporal–occipital pole or AT–OP distance). To verify the accuracy of this method of using the tip of the fossa as a surrogate for the temporal pole, measures of the AT–OP distance were obtained in the non-resected hemisphere, using the existing temporal pole to mark the anterior temporal position. *t*-tests showed no significant bias in the AT–OP estimates between the intact and resected hemispheres, despite the differences in methods.

Visual field assessment

All patients had postoperative Goldmann perimetry carried out by a consultant ophthalmologist (J.A.), at least 3 months after surgery, in order to decrease the likelihood of confounding temporary VFDs from brain oedema. The ophthalmologist was blinded to the results of tractography, and estimates of resection size. Perimetry was performed in a standardized fashion for each eye separately generating three isopters with the V4e, I4e and I2e targets. The results of perimetry were quantified using a previously described method to calculate the proportion of area lost for the three isopters (Barton *et al*., 2005). These values were averaged across all three isopters, and then across both eyes to give an overall estimate of visual field loss. Conventional isopter plotting will typically conceal the cartographic distortion error, which is inherent in the transposition of the isopter on the curved perimeter bowel onto flat, polar, azimuthal visual field charts (Frisen, 1970; Kirkham and Meyer, 1981). This can lead to the underestimation of visual field area, and any visual field loss measured by planimetry. However, this error should be similar across subjects for each isopter, and should therefore not affect the relationship between the anterior extent of Meyer's loop and visual field loss. Furthermore, because the central field is represented in all three isopters, unlike the periphery which is covered by fewer isopters, this method should weight the central field more than the peripheral field. Therefore, this should account for some of the physiological central magnification present in the optic nerve, which can confound any linear relationship between visual field loss, and axonal loss (Curcio and Allen, 1990).

Statistical analysis

All statistical analysis was carried out using SPSS v14 (SPSS Inc., Chicago, USA). Group differences for age were determined by a one-way analysis of variance (ANOVA), and gender distribution was assessed using the Pearson's χ^2 test.

The relationship of interest was between the VFD, and the anterior extent of Meyer's loop. The size of the temporal lobe resection is a potential confounder of this relationship. Multiple regression analysis was therefore specified to model the relationship between VFD as a dependent variable, and ML–TP and resection size as independent variables. Both variables were entered into the model simultaneously. Partial regression plots were inspected for outliers and heteroskedacity, and residuals tested for normality using the Shapiro–Wilkes test. The Durbin–Watson test was used to test for the independence of the error terms. In view of the fact that any linear relationship between the anterior extent of Meyer's loop, and visual field loss may be confounded by the lack of a 'one-to-one' relationship between field loss and axonal numbers, we also carried out a categorical analysis of the data using a 2×2 contingency table, and Fisher's exact test.

We also carried out a two way mixed ANOVA with one between subjects factor [group – controls or TLE (both left and right)] and one within subjects factor (hemisphere – left or right), to test for the effect of group, hemisphere, or an interaction between group and hemisphere, on ML–TP. Prior to this analysis it was first verified that all parameters were normally distributed using the Shapiro–Wilkes test for normal distribution.

Results

Demographic analysis

There was no significant difference in the mean age or gender distribution of participants in the three groups (controls, left TLE, right TLE).

Resection size and VFDs

Right ATLRs averaged 34% of the TP–OP distance, compared with 31% for left ATLR (Table 2), though this difference was not statistically significant. Six of the 11 patients undergoing a left ATLR suffered postoperative VFDs, compared with 3 of the 10 patients undergoing a right ATLR. Three of these patients (two post-left ATLR, one post-right ATLR) would fail DVLA criteria to be granted a UK driving license. Although left ATLRs tended to result in bigger VFDs than right ATLRs (mean of 26% compared with 22% of superior contralateral quadrant, averaged across three isopters and both eyes) this was not statistically significant. The postoperative VFDs tended to be incongruous, with loss of field extending from the vertical meridian towards the horizontal meridian, in keeping with previous reports (Barton *et al*., 2005) (Fig. 4).

Table 2 Results of quantitative analysis of Meyer's loop

Group	L ML–TP (mm)	R ML–TP (mm)	L ML–TH (mm)	R ML–TH (mm)	Resection size (%AT–OP)	VFD (% superior quadrant)
L TLE	32 (2); 24 to 39	35 (1); 28 to 41	2 (1); −4 to 9	−3 (1); −15 to 2	0.31 (0.02); 0.15 to 0.41	26 (9); 0 to 87
R TLE	35 (1); 30 to 43	34 (2); 26 to 43	−1 (2); −8 to 8	1 (1); −4 to 8	0.34 (0.01); 0.28 to 0.40	22 (11); 0 to 76
Controls	34 (1); 24 to 41	36 (1); 32 to 47	2 (1); −4 to 9	−1 (1); −11 to 4		

VFD expressed as a percentage of superior quadrantic field. This is calculated by averaging the proportion of quadrantic field loss across three isopters (V4e, I4e and I2e) and both eyes as measured by Goldmann perimetry. Values are given as mean (SE); range.

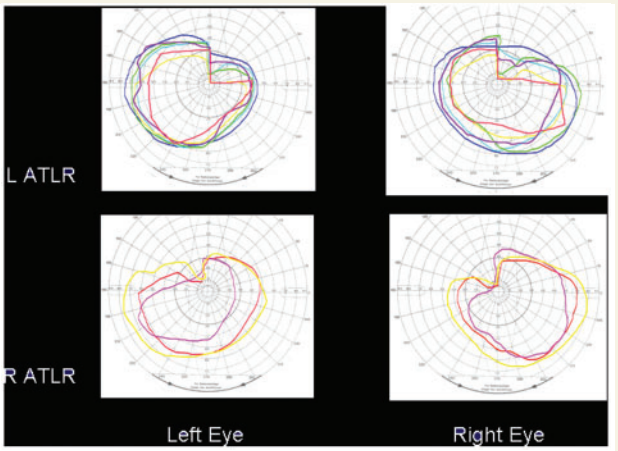

Figure 4 Representative VFDs in one isopter only (I4e). Each colour represents a single patient. The range of magnitude of VFDs averaged across all three isopters was 22–87% of the superior contralateral quadrant in patients undergoing left ATLR, and 47–76% in patients undergoing right ATLR.

Qualitative analysis

In all subjects, the anterior portion of Meyer's loop typically passed over the roof of the temporal horn (Fig. 5A), before then turning posteriorly to pass along the lateral inferior aspect of the temporal horn (Fig. 5B). Fibres then passed laterally to the occipital horn of the ventricle (Fig. 5C), and terminated in the calcarine sulcus and occipital pole (Fig. 5D).

Quantitative analysis

In patients, the range of ML–TP was 24–43 mm (mean 34 mm), and the range of ML–TH was −15 to +9 mm (mean 0 mm). In controls, the range of ML–TP was 24–47 mm (mean 35 mm), and the range of ML–TH was −11 to +9 mm (mean 0 mm) (Table 2). Following multiple regression analysis both ML–TP ($\beta = -0.80$, $P < 0.001$) and size of ATLR ($\beta = 0.41$, $P < 0.05$) were significant predictors of post-operative VFDs (adjusted $r^2 = 0.63$). Partial residual plots showed homoskedacity without significant outliers (Fig. 6), and residuals from the analysis were normally distributed. There was no correlation between residual terms.

The ANOVA analysis revealed a trend towards the left ML–TP distance being smaller than the right ML–TP across all groups ($P = 0.07$). There was no interaction between groups and sides.

Fisher's test revealed a significant association between the anterior extent of Meyer's loop and whether a patient suffered a severe (>50%) quadrantic VFD $\chi^2(1) = 5.19$, $P = 0.01$ (two-tailed); if the anterior extent of Meyer's loop was <35 mm from the temporal pole, patients were more likely to suffer severe VFDs, irrespective of the size of resection. The threshold values used to categorize the data were chosen because 50% represented the midpoint of the VFD range and was regarded as the minimum cut-off for further binocular testing if seizure free patients wished to drive, and 35 mm represented the approximate midpoint of the range of ML–TP distances found across controls and patients (Table 2).

Discussion

This study demonstrates the parcellation of the optic radiation and Meyer's loop using probabilistic tractography applied to diffusion tensor data acquired at 3T. The anatomy of the tracts that have been obtained using this technique is comparable to the results described in dissection based studies. In patients, the range of ML–TP was found to be 24–43 mm (mean 34 mm), while the range of ML–TH was −15 to 9 mm (mean 0 mm). While there was no statistically significant difference in the anterior extent of the right and left optic radiations across patients and controls, there was a trend toward the left optic radiation extending more anteriorly than the right optic radiation in both patients and controls. Because the optic radiation and its anterior extent could not previously be visualized with conventional, clinical MRI sequences, this information was not incorporated into studies investigating the relationship between MRI based volumetric assessment of resection size and VFDs. Using tractography we have now demonstrated that both the size of ATLR, and the anterior extent of the optic radiation are predictors of the occurrence and severity of postoperative VFDs.

Studies of Meyer's loop

Following the original description just over one century ago by Meyer and Archambault, of the 'peculiar detour of the ventral portion of the geniculocalcarine path' (Archambault, 1906; Meyer, 1907), there has been considerable interest in the anatomy and pathology of the optic radiation. Initial studies were based on patients with tumours (Cushing, 1922) or gunshot wounds to the temporal lobe (Spalding, 1952) With the introduction of the ATLR for refractory temporal lobe epilepsy and appreciation of the occurrence of postoperative VFDs, interest in the optic radiation and Meyer's loop has increased significantly. There has been considerable heterogeneity as to the incidence of VFDs following ATLR. While some studies have reported a correlation between extent of resection and the presence/absence of a VFD (Falconer and Wilson, 1958; Jensen and Seedorff, 1976; Katz *et al*., 1989; Hughes *et al*., 1999), others have not found this to be the case (Marino and Rasmussen, 1968; Babb *et al*., 1982; Tecoma *et al*., 1993). Even fewer studies have demonstrated a correlation between the severity of a resulting VFD and extent of resection (Krolak-Salmon *et al*., 2000). Moreover, in studies comparing selective with *en bloc* temporal lobe resections, there again appeared to be little correlation with either the frequency or extent of VFDs (Egan *et al*., 2000; Nilsson *et al*., 2004). While patient selection, and the methods used for both surgery and VFD assessment have changed over time and differ between studies, the variability in the anterior extent of Meyer's loop is an additional confounding factor.

Studies assessing the anterior extent of Meyer's loop and its anatomical relationships can be broadly divided into three

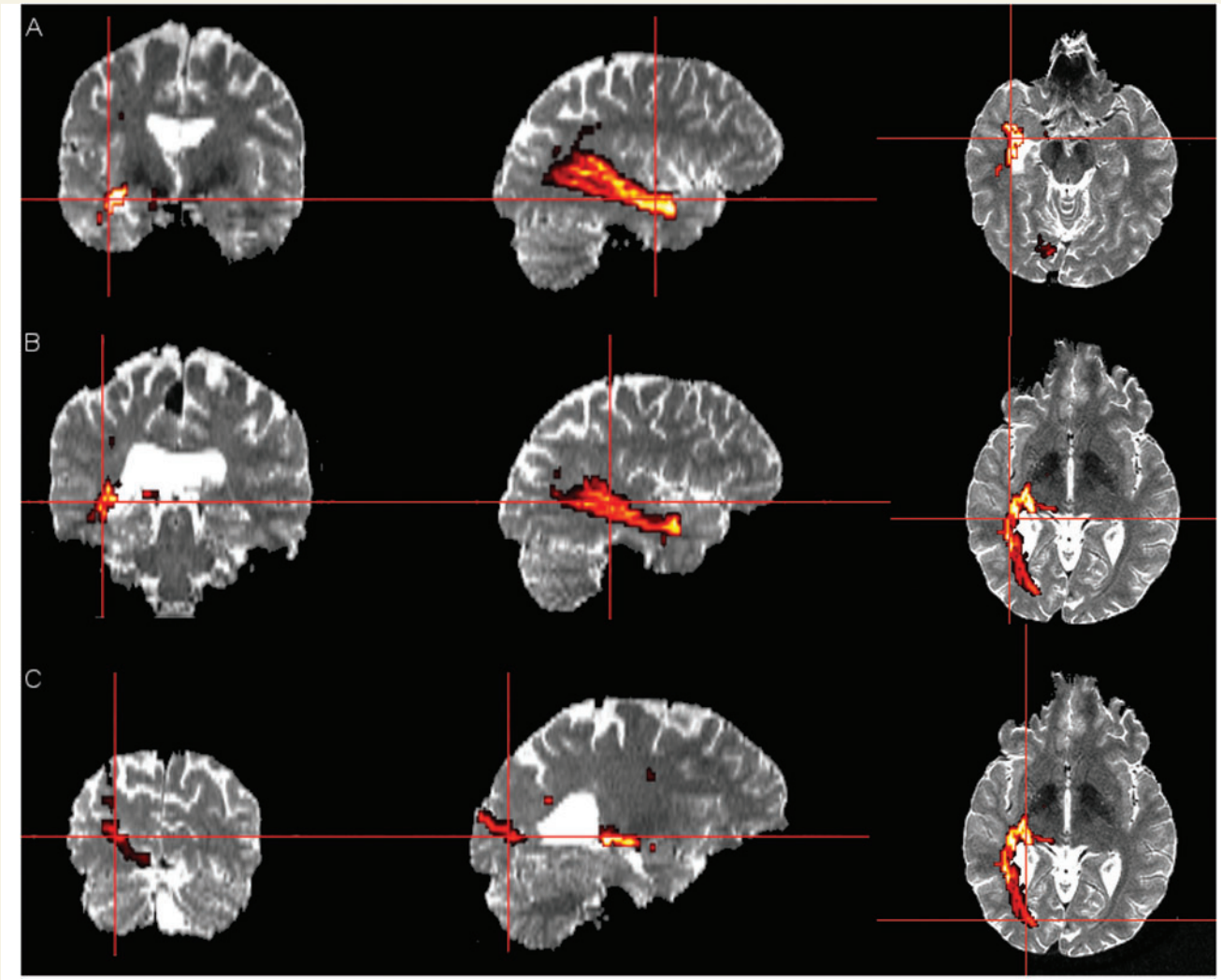

Figure 5 Representative tract of the optic radiation of a single patient overlaid on a distortion matched HR-EPI image. (**A**) Anterior portion of Meyer's loop passing over the roof of the temporal horn. (**B**) Along the lateral inferior aspect of the temporal horn. (**C**) Termination in the calcarine sulcus, and occipital pole.

groups. The first and largest group of studies have used estimates of both resection size and the severity of postoperative VFDs, in order to deduce the anatomy of the optic radiation (Table 3). Penfield first stated over 50 years ago, that lesions that were <60 mm from the temporal tip were not likely to produce a field deficit (Penfield, 1954). Subsequent studies, however, have gradually reduced this estimate. Older studies which used intra-operative measurements are likely to have overestimated resection size (Awad *et al*., 1989), and therefore underestimated the anterior extent of Meyer's loop.

A smaller group of studies have used the Klingler dissection technique in the cadaveric brains of previously healthy subjects, in order to investigate the anatomical relationships of Meyer's loop. The largest of these studies reported an average distance of 27 mm for ML–TP, but at the same time emphasized the variability between subjects (Ebeling and Reulen, 1988). Other dissection-based studies demonstrated that Meyer's loop tends to cap the temporal horn, and all reported ML–TP distances which were smaller than those found in the first group of studies (Table 4). In contrast to resection based assessments, however, these studies may be susceptible to overestimations of the anterior extent of Meyer's loop. It can be difficult to delineate accurately the anterior extent of the optic radiation using micro-dissection techniques, particularly amongst a dense network of neighbouring fibres that includes the uncinate fasciculus, occipito-frontal fasciculus, anterior commissure and thalamic fibre tracts (Yasargil *et al*., 2004).

The final group of studies that have assessed the optic radiation have incorporated digital photography, and computer reconstructions of block images of cryosectioned brain (Burgel *et al*., 1999; Kier *et al*., 2004). While these studies have tended not to derive measurements of the anatomical relationships of Meyer's loop, they do describe the anatomy of the optic radiation, and its relationship to the temporal horn. Burgel *et al*. (1999) studied 10 control brains, and found in all cases that Meyer's loop capped the temporal horn. On the other hand, Kier *et al*.

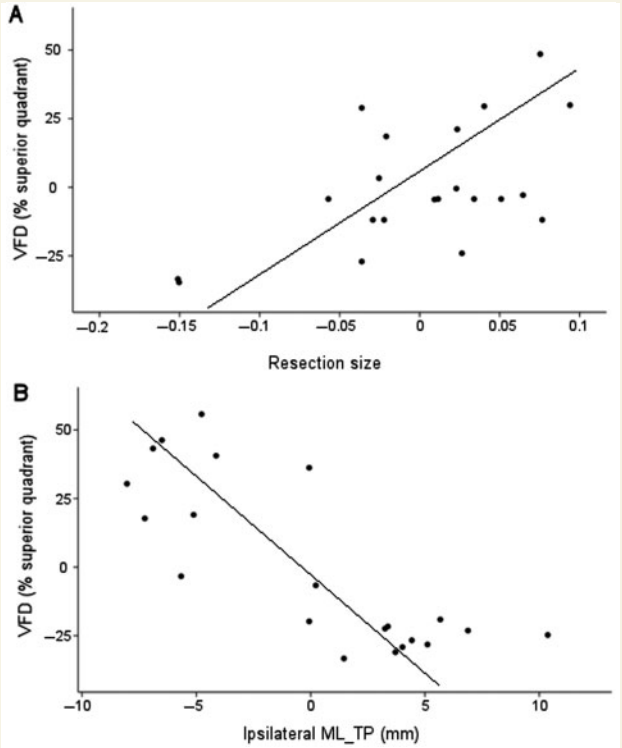

Figure 6 Partial residual plots demonstrating the variance in ML–TP and resection size attributable to the model. (**A**) Extent of VFD against corrected anterior–posterior extent of temporal lobe resection, showing positive correlation $r^2 = 0.63$. (**B**) Extent of VFD against distance of tip of Meyer's loop to temporal pole, showing inverse correlation $r^2 = -0.80$.

(2004) studied the temporal stem of a single normal brain, and reported that Meyer's loop was posterior to the temporal horn.

Tractography and Meyer's loop

The most recent development in the study of the optic radiation has been the application of diffusion based tractography. This technique has the advantage over post-mortem studies of allowing the study of the optic radiation and its anatomical relationships *in vivo*. Most studies to date have incorporated small numbers of subjects and patients, and have used deterministic algorithms on diffusion data acquired at 1.5T. Yamamoto *et al*. (2005) assessed five healthy controls, and reported an ML–TP range of 33–40 mm (mean 37 mm), and that Meyer's loop capped the temporal horn (range 3.7–4.3 mm, mean 4 mm). Nilsson *et al*. (2007) studied two patients undergoing temporal lobe surgery and seven controls. They reported that the ML–TP range was 34–51 mm (mean 44 mm) in controls and 40–51 mm (mean 45.5 mm) in patients. They also reported that Meyer's loop did not reach the temporal horn in any of the subjects studied. Both these studies place Meyer's loop more posteriorly than reported in the current investigation. Deterministic tractography, however, can have difficulty in areas of crossing/kissing fibres such as Meyer's loop, and may therefore underestimate the anterior extent of Meyer's loop. For this reason, a modified approach was adopted by Taoka *et al*. (2008) in a study of 14 patients undergoing temporal lobe surgery. Although a deterministic method was used, the uncinate fasciculus (UF) was initially tracked, and used to define the anterior extent of ML. The ML–TP distances reported were less (mean 36.6 mm, range 30–43.2 mm) than the previous studies, but again smaller than those reported in this study and the other groups of studies described above. Taoka *et al*. also reported a distance of 0 mm between the uncinate fasciculus and ML in at least seven cases. It is therefore likely that despite the use of an anterior marker, the deterministic approach may have had difficulty in resolving neighbouring white matter bundles.

Probabilistic multi-fibre tractography applied to diffusion MRI data acquired at 3T may be better able to cope with crossing and kissing fibres than deterministic models because it allows many more possible local pathway orientations for each DTI sample point. Consequently, it is therefore less likely to underestimate the anterior extent of Meyer's loop. This has been eloquently demonstrated by Sherbondy *et al*. who used a probabilistic multitensor approach with the use of priors, in a study of the optic radiation in 8 healthy volunteers (Sherbondy *et al*., 2008). They found that the most anterior extent of Meyer's loop was 28 ± 3 mm posterior to the temporal pole, with a population range of 10 mm. The results reported in the current study are similar to this, and another recently published tractography study by Chen *et al*. (2009) who found that the mean distance of ML–TP was 32 mm with a range of 21–52 mm. The results of the current study are also concordant with the largest reported dissection-based study (Ebeling and Reulen, 1988) (ML–TP = 22–37 mm, mean = 27 mm and ML–TH = −5 to 10 mm, mean = 5mm), and the most recent resection VFD-based study by Barton *et al*. (2005) (ML–TP $\geqslant$ 24 mm, ML–TH 4–8 mm). By measuring the resection size, as well as the anterior extent of Meyer's loop, we have also demonstrated that VFDs following ATLR are directly proportional to both variables, although the latter variable appears to be the more important factor. The upper limit of ML–TP that was associated with a VFD was 32 mm, and the categorical analysis demonstrates that patients with an ML–TP distance of <35 mm from the temporal pole are at greater risk of VFDs than those with ML–TP distances >35 mm from the pole, regardless of resection size. The distance from the temporal pole to the temporal horn was relatively constant in this study (mean = 34 mm) and in agreement with other studies (Ebeling and Reulen, 1988; Nilsson *et al*., 2007). The cut-off of 35 mm may therefore represent the point at which a lateral or superior surgical approach causes large enough disruption of fibres covering the roof of the temporal horn so as to cause a significant VFD. Taoka *et al*. reported similar findings, but used an ANOVA analysis to compare the mean distance from the anterior limit of Meyer's loop to the posterior limit of resection, between categories of patients with varying severity of VFDs. The mean distance was calculated by subtracting the distance from the temporal tip to the posterior resection margin as measured on a postoperative T1 image, from the anterior limit of Meyer's loop as measured on a preoperative $b = 0$ image. Patients with the most severe VFDs, typically had larger

Table 3 Studies on temporal lobe surgery resection sizes, VFDs and inferred anatomy of the optic radiation

Reference	Numbers of patients undergoing surgery	Method of field assessment	VFD (magnitude as percent superior contralateral quadrant)	Anatomical inferences and ML
Bjork *et al*. (1957)	26 ATLR	Goldmann	96% (partial)	ML–TP ⩾ 30 mm ML caps TH
Falconer *et al*. (1958)	18 (right) 32 (left) ATLR	Bjerrum	64% (complete) 36% (incomplete)	ML–TP ⩾ 45 mm ML caps TH
Van Buren *et al*. (1958)	1 ATLR	Perimetry (not specified) and Tangent	80% (not specified)	ML does not cap TH
Wendland *et al*. (1960)	24 ATLR	Not specified	63% (complete) 37% (partial)	ML–TP ⩾ 50 mm
Marino *et al*. (1968)	25 (right) 25 (left) ATLR	Aimark and Tangent	14% (complete) 52% (incomplete)	ML–TP ⩾ 40 mm ML does not cap TH
Hughes *et al*. (1999)	12 (left) 20 (right) ATLR	Humphrey	97% ('predominantly incomplete')	ML–TP ⩾ 40 mm
Krolak-Salmon *et al*. (2000)	11 (left) 7 (right) ATLR	Automated Static Perimetry	28% (mild) 28% (moderate) 28% (total)	ML–TP ⩾ 20 mm ML caps TH
Nilsson *et al*. (2004)	50 ATLR and modified ATLR	Goldmann	50% across both groups (no significant difference between groups)	ML–TP ⩾ 18 mm
Barton *et al*. (2005)	16 (left) 13 (right) ATLR	Goldmann	100% (average loss of 63% of a quadrant)	ML–TP ⩾ 24 mm ML caps TH (by 4 mm to 8 mm)

ML = Meyer's loop; TH = temporal horn.

Table 4 Dissection based studies of the optic radiation

Reference	No. of cadaveric hemispheres studied	Anatomical inferences and ML
Ebeling *et al*. (1988)	50 (controls)	ML–TP = 22mm to 37mm (mean = 27mm) ML–TH = − 5 mm to 10mm (mean = 5mm)
Sincoff *et al*. (2004)	20 (controls)	ML caps TH
Rubino *et al*. (2005)	40 (controls)	ML–TP = 22mm to 30mm (mean = 25mm) ML–TH = 1mm to 3mm (mean = 2mm)
Choi *et al*. (2006)	10 (controls)	ML–TP = 28mm to 34mm (mean = 31.4mm) ML caps TH
Peltier *et al*. (2006)	20 (controls)	ML–TP = 15–30mm ML ⩽ 5mm anterior to TH

ML = Meyer's loop; TH = temporal horn.

values suggesting greater overlap between Meyer's loop and the area of resection. This approach, however, does not lend itself to pre-surgical risk assessment, and may be problematic because the measurements used are susceptible to distortion artefact differences between the differing MRI sequences. By using a linear regression analysis incorporating the resection size and the anterior extent of Meyer's loop, based on the T1 and $b = 0$ images, respectively, the distortion errors should be similar in each subject in the current study.

The discovery of a trend towards the left optic radiation extending more anteriorly compared to the right optic radiation across all groups, is a novel finding. This may partly explain the higher incidence of VFDs in left compared to right ATLRs, despite the fact that larger resections typically occurred on the non-dominant, right side. A recent study in this Centre of 105 patients who underwent ATLR has demonstrated similar findings (Jeelani *et al*., 2007). After accounting for the extent of tissue resections, left-sided resections were found to carry significantly greater risk of VFDs compared with right-sided resections (Odds Ratio 4.43, $P = 0.01$). The authors concluded that the geniculocalcarine tract extended further anteriorly on the left compared to the right-sided tract. Histological based studies have also reported leftward asymmetry in the optic radiation (Burgel *et al*., 1999), concordant with the findings reported here.

Limitations

The retrospective nature and the lack of full blinding are shortcomings of this study. To compensate for this, we used strict anatomical rules for the placement of start regions, as well as graphical displays to interpret the appropriate placement of fronto-temporal exclusion masks. Furthermore, we demonstrated that the intra-observer variability in the assessment of ML–TP was minimal, which lends confidence to the reproducibility of our findings. Although patients did not have preoperative perimetry, all had normal visual fields to confrontation testing, and none had symptoms to suggest field deficits prior to surgery. The two patients with cavernomas had normal visual fields postoperatively. Furthermore, visual fields are typically normal in patients with non-expanding lesions of the temporal lobe, as reported in other

studies (Hughes *et al*., 1999; Krolak-Salmon *et al*., 2000). Although the methods used for resection estimation were based on previously validated studies (Barton *et al*., 2005), more sophisticated methods that take into account postoperative gliosis (Awad *et al*., 1989), may enable better modelling of the relationship between the anterior extent of Meyer's loop and VFDs. Similarly, development of more refined perimetric analysis methods should enable better understanding of this relationship. In this study we have used a relatively simple model that considers damage to the optic radiation in only the coronal plane. Because the anterior tip of Meyer's loop is the area that will typically incur the most damage after ATLR, damage in this plane should broadly correlate with postoperative VFDs. However, as resection is typically at an oblique angle to the temporal pole, and can sometimes involve the removal of parts of the para-hippocampal and fusiform gyri, in future studies it will be important to assess any damage to the optic radiation in other planes.

The remaining limitations of this study are common to most tractography based investigations. The resolution of tractography images is several orders of magnitude lower than the nerve bundles under examination. A single voxel contains numerous fibre populations, some of which may be kissing or crossing. The multiple fibre population model, and probabilistic tractography approach employed in this study, may be able to cope with this better than deterministic approaches. As methodological developments occur in spatial resolution, diffusion modelling (e.g. diffusion spectrum imaging), and tractography algorithms, these limitations should prove less of a problem. In the interim, anatomical validation of the derived white matter tracts is crucial, particularly as tractography is a subjective process, dependent on user defined parameters. Though this technique is able to demonstrate the relationship between the anatomy of Meyer's loop and VFDs, the tracts themselves are 'virtual' representations of the underlying white matter. Kamada *et al*. demonstrated that real-time, perioperative visual evoked potentials confirmed the accuracy of tractography of the optic radiation (Kamada *et al*., 2005). This, together with the qualitative similarity of the tracts in this study to those described in dissection studies, lends support to the anatomical validity of tractography derived images of the optic radiation. In the future, validation of the tractography derived anatomy of the visual pathway may also be aided by the implementation of a combination of manganese enhanced MRI and diffusion tensor tractography in animal models (Yamada *et al*., 2008).

Conclusion

In this study we have demonstrated the feasibility of tractography of the optic radiation in patients undergoing temporal lobe resections. By measuring the anatomical relationships of Meyer's loop we have shown that it is possible to predict the occurrence and extent of postoperative VFDs for a given resection size. This information could prove useful in the preoperative advice given to patients regarding the risk of VFD. By using the information derived from the categorical analysis, it may be possible to stratify patients into groups at high or low risk for VFDs. The definitive goal of tractography of the optic radiation is its integration into stereo-navigational systems together with T_1-weighted anatomical images. However, differing geometric distortions between EPI- and T1-based images makes accurate co-registration, particularly in areas such as the temporal lobe, difficult. Furthermore, perioperative brain shift can complicate the nature of the anatomical relationships derived preoperatively between the temporal pole and Meyer's loop. The use of alternative landmarks less prone to brainshift, such as the lateral geniculate body or brainstem, may prove more useful perioperatively. Ultimately, the solution to both of these problems will encompass the use of real-time, intra-operative scanning. However, in view of the length of time needed in this study for the acquisition and tractography processing of diffusion tensor data, the feasibility of these advances depends on the development of robust and rapid diffusion acquisition schemes, and tractography algorithms (Chen *et al*., 2009), that may be co-registered with higher definition tractography that has been acquired preoperatively. This is an area we plan to explore in future studies.

Acknowledgements

We are grateful to our patients and control subjects for their enthusiastic participation, and to Pip Bartlett, Elaine Williams and Jane Burdett for excellent MRI acquisitions.

Funding

Wellcome Trust (Programme grant 067176); Big Lottery fund; Wolfson Trust and National Society for Epilepsy (NSE MRI scanner); Department of Health's National Institute for Health Research, Biomedical Research Centres funding scheme (to UCLH/UCL, where the work was undertaken).

References

Alexander DC, Barker GJ, Arridge SR. Detection and modeling of non-Gaussian apparent diffusion coefficient profiles in human brain data. Magn Reson Med 2002; 48: 331–40.

Archambault L. Le faisceau longitudinal inferieur et le faisceau optique central: Quelques considerations sur les fibers d'association du cerveau. Rev Neurol 1906; 4: 1206.

Awad IA, Katz A, Hahn JF, Kong AK, Ahl J, Luders H. Extent of resection in temporal lobectomy for epilepsy. I. Interobserver analysis and correlation with seizure outcome. Epilepsia 1989; 30: 756–62.

Babb TL, Wilson CL, Crandall PH. Asymmetry and ventral course of the human geniculostriate pathway as determined by hippocampal visual evoked potentials and subsequent visual field defects after temporal lobectomy. Exp Brain Res 1982; 47: 317–28.

Barton JJ, Hefter R, Chang B, Schomer D, Drislane F. The field defects of anterior temporal lobectomy: a quantitative reassessment of Meyer's loop. Brain 2005; 128: 2123–33.

Basser PJ. Inferring microstructural features and the physiological state of tissues from diffusion-weighted images. NMR Biomed 1995; 8: 333–44.

Bassi L, Ricci D, Volzone A, Allsop JM, Srinivasan L, Pai A, et al. Probabilistic diffusion tractography of the optic radiations and visual

function in preterm infants at term equivalent age. Brain 2008; 131: 573–82.
Behrens TE, Woolrich MW, Jenkinson M, Johansen-Berg H, Nunes RG, Clare S, et al. Characterization and propagation of uncertainty in diffusion-weighted MR imaging. Magn Reson Med 2003; 50: 1077–88.
Boulby PA, Symms M, Barker GJ. Distortion matching echo planar images at different field strengths. In: ISMRM 13th Scientific Meeting & Exhibition, Miami, FL, USA, 2005. p. 2276.
Burgel U, Schormann T, Schleicher A, Zilles K. Mapping of histologically identified long fiber tracts in human cerebral hemispheres to the MRI volume of a reference brain: position and spatial variability of the optic radiation. Neuroimage 1999; 10: 489–99.
Chen X, Weigel D, Ganslandt O, Buchfelder M, Nimsky C. Prediction of visual field deficits by diffusion tensor imaging in temporal lobe epilepsy surgery. Neuroimage 2009; 45: 286–97.
Ciccarelli O, Toosy AT, Hickman SJ, Parker GJ, Wheeler-Kingshott CA, Miller DH, et al. Optic radiation changes after optic neuritis detected by tractography-based group mapping. Hum Brain Mapp 2005; 25: 308–16.
Cook PA, Alexander DC, Parker GJ. Modelling noise-induced fibre-orientation error in diffusion-tensor MRI. IEEE Int Symp Biomed Imaging 2004; 332–5.
Cook PA, Bai Y, Nedjati-Gilani S, Seunarine KK, Hall MG, Parker GJ, *et al*. Camino: open-source diffusion-MRI reconstruction and processing. In: 14th Scientific Meeting of the International Society for Magentic Resonance in Medicine, Seattle, WA, USA; 2006. p. 2759.
Cook PA, Symms M, Boulby PA, Alexander DC. Optimal acquisition orders of diffusion-weighted MRI measurements. J Magn Reson Imaging 2007; 25: 1051–8.
Curcio CA, Allen KA. Topography of ganglion cells in human retina. J Comp Neurol 1990; 300: 5–25.
Cushing H. Distortions of visual fields in cases of brain tumour. Brain 1922; 44: 341.
Duncan JS. Imaging and epilepsy. Brain 1997; 120 (Pt 2): 339–77.
Ebeling U, Reulen HJ. Neurosurgical topography of the optic radiation in the temporal lobe. Acta Neurochir (Wien) 1988; 92: 29–36.
Egan RA, Shults WT, So N, Burchiel K, Kellogg JX, Salinsky M. Visual field deficits in conventional anterior temporal lobectomy versus amygdalohippocampectomy. Neurology 2000; 55: 1818–22.
Falconer MA, Wilson JL. Visual field changes following anterior temporal lobectomy: their significance in relation to Meyer's loop of the optic radiation. Brain 1958; 81: 1–14.
Frisen L. The cartographic deformations of the visual field. Ophthalmologica 1970; 161: 38–54.
Hughes TS, Abou-Khalil B, Lavin PJ, Fakhoury T, Blumenkopf B, Donahue SP. Visual field defects after temporal lobe resection: a prospective quantitative analysis. Neurology 1999; 53: 167–72.
Jeelani NU, Harkness W, Zrinzo K, Poon T, Kabasele P, Galton M, et al. 'Do what is right and think about what is left'—hemispheric asymmetry in the optic pathway radiations in temporal lobe surgery. Epilepsia 2007; Abstract 1.290.
Jensen I, Seedorff HH. Temporal lobe epilepsy and neuro-ophthalmology. Ophthalmological findings in 74 temporal lobe resected patients. Acta Ophthalmol (Copenh) 1976; 54: 827–41.
Kamada K, Todo T, Morita A, Masutani Y, Aoki S, Ino K, et al. Functional monitoring for visual pathway using real-time visual evoked potentials and optic-radiation tractography. Neurosurgery 2005; 57: 121–7.
Katz A, Awad IA, Kong AK, Chelune GJ, Naugle RI, Wyllie E, et al. Extent of resection in temporal lobectomy for epilepsy. II. Memory changes and neurologic complications. Epilepsia 1989; 30: 763–71.
Kier EL, Staib LH, Davis LM, Bronen RA. MR imaging of the temporal stem: anatomic dissection tractography of the uncinate fasciculus, inferior occipitofrontal fasciculus, and Meyer's loop of the optic radiation. Am J Neuroradiol 2004; 25: 677–91.
Kirkham TH, Meyer E. Visual field area on the Goldmann hemispheric perimeter surface. Correction of cartographic errors inherent in perimetry. Curr Eye Res 1981; 1: 93–9.
Krolak-Salmon P, Guenot M, Tiliket C, Isnard J, Sindou M, Mauguiere C, et al. Anatomy of optic nerve radiations as assessed by static perimetry and MRI after tailored temporal lobectomy. Br J Ophthalmol. 2000; 84: 884–9.
Manji H, Plant GT. Epilepsy surgery, visual fields, and driving: a study of the visual field criteria for driving in patients after temporal lobe epilepsy surgery with a comparison of Goldmann and Esterman perimetry. J Neurol Neurosurg Psychiatry 2000; 68: 80–2.
Marino R Jr, Rasmussen T. Visual field changes after temporal lobectomy in man. Neurology 1968; 18: 825–35.
Meyer A. The connections of the occpital lobes and the present status of the cerebral visual affections. Trans Assoc Am Phys 1907; 22: 7–30.
Moran NF, Lemieux L, Maudgil D, Kitchen ND, Fish DR, Shorvon SD. Analysis of temporal lobe resections in MR images. Epilepsia 1999; 40: 1077–84.
Mori S, van Zijl PC. Fiber tracking: principles and strategies - a technical review. NMR Biomed 2002; 15: 468–80.
Nilsson D, Malmgren K, Rydenhag B, Frisen L. Visual field defects after temporal lobectomy — comparing methods and analysing resection size. Acta Neurol Scand 2004; 110: 301–7.
Nilsson D, Starck G, Ljungberg M, Ribbelin S, Jonsson L, Malmgren K, et al. Intersubject variability in the anterior extent of the optic radiation assessed by tractography. Epilepsy Res 2007; 77: 11–16.
Oldfield RC. The assessment and analysis of handedness: the Edinburgh inventory. Neuropsychologia 1971; 9: 97–113.
Parker GJ, Alexander DC. Probabilistic Monte Carlo based mapping of cerebral connections utilising whole-brain crossing fibre information. Lect Notes Comput Sci 2003; 2732: 684–95.
Parker GJ, Haroon HA, Wheeler-Kingshott CA. A framework for a streamline-based probabilistic index of connectivity (PICo) using a structural interpretation of MRI diffusion measurements. J Magn Reson Imaging 2003; 18: 242–54.
Penfield W. Temporal lobe epilepsy. Br J Surg 1954; 41: 337–43.
Powell HW, Parker GJ, Alexander DC, Symms MR, Boulby PA, Wheeler-Kingshott CA, et al. MR tractography predicts visual field defects following temporal lobe resection. Neurology 2005; 65: 596–9.
Powell HW, Parker GJ, Alexander DC, Symms MR, Boulby PA, Wheeler-Kingshott CA, et al. Hemispheric asymmetries in language-related pathways: a combined functional MRI and tractography study. Neuroimage 2006; 32: 388–99.
Ray A, Pathak-Ray V, Walters R, Hatfield R. Driving after epilepsy surgery: effects of visual field defects and epilepsy control. Br J Neurosurg 2002; 16: 456–60.
Semah F, Picot MC, Adam C, et al. Is the underlying cause of epilepsy a major prognostic factor for recurrence? Neurology 1998; 51: 1256–62.
Sherbondy AJ, Dougherty RF, Napel S, Wandell BA. Identifying the human optic radiation using diffusion imaging and fibre tractography. J Vision 2008; 8: 1–11.
Spalding JM. Wounds of the visual pathway. I. The visual radiation. J Neurol Neurosurg Psychiatry 1952; 15: 99–109.
Taoka T, Sakamoto M, Nakagawa H, Nakase H, Iwasaki S, Takayama K, et al. Diffusion tensor tractography of the meyer loop in cases of temporal lobe resection for temporal lobe epilepsy: correlation between postsurgical visual field defect and anterior limit of meyer loop on tractography. AJNR Am J Neuroradiol 2008; 29: 1329–34.
Taylor DC, McMacKin D, Staunton H, Delanty N, Phillips J. Patients' aims for epilepsy surgery: desires beyond seizure freedom. Epilepsia 2001; 42: 629–33.
Tecoma ES, Laxer KD, Barbaro NM, Plant GT. Frequency and characteristics of visual field deficits after surgery for mesial temporal sclerosis. Neurology 1993; 43: 1235–8.

Wheeler-Kingshott CA, Hickman SJ, Parker GJ, Ciccarelli O, Symms MR, Miller DH, et al. Investigating cervical spinal cord structure using axial diffusion tensor imaging. Neuroimage 2002; 16: 93–102.

Wiebe S, Blume WT, Girvin JP, Eliasziw M. A randomized, controlled trial of surgery for temporal-lobe epilepsy. N Engl J Med 2001; 345: 311–8.

Wieser HG, Blume WT, Fish D, Goldensohn E, Hufnagel A, King D, et al. ILAE Commission Report. Proposal for a new classification of outcome with respect to epileptic seizures following epilepsy surgery. Epilepsia 2001; 42: 282–6.

Woermann FG, Barker GJ, Birnie KD, Meencke HJ, Duncan JS. Regional changes in hippocampal T2 relaxation and volume: a quantitative magnetic resonance imaging study of hippocampal sclerosis. J Neurol Neurosurg Psychiatry 1998; 65: 656–64.

Yamada M, Momoshima S, Masutani Y, Fujiyoshi K, Abe O, Nakamura M, et al. Diffusion-tensor neuronal fiber tractography and manganese-enhanced MR imaging of primate visual pathway in the common marmoset: preliminary results. Radiology 2008; 249: 855–64.

Yamamoto T, Yamada K, Nishimura T, Kinoshita S. Tractography to depict three layers of visual field trajectories to the calcarine gyri. Am J Ophthalmol 2005; 140: 781–5.

Yasargil MG, Ture U, Yasargil DC. Impact of temporal lobe surgery. J Neurosurg 2004; 101: 725–38.